Available online at www.sciencedirect.com
ScienceDirect
Ceramics International 37 (2011) 3161–3165
CERAMICS INTERNATIONAL
www.elsevier.com/locate/ceramint

Synthesis and characterization of Cu-doped ceria nanopowders

B.Z. Matović [a], D.M. Bučevac [a], M. Rosić [a], B.M. Babić [a,*], Z.D. Dohcević-Mitrović [b], M.B. Radović [b], Z.V. Popović [b]

[a] *Institute of Nuclear Sciences "Vinča", Belgrade University, P.O. Box 522, 11000 Belgrade, Serbia*
[b] *Institute of Physics, Centre for Solid State Physics and New Materials, Belgrade University, Pregrevica 118, 11080 Belgrade, Serbia*

Received 4 October 2010; received in revised form 20 December 2010; accepted 26 March 2011
Available online 26 May 2011

Abstract

Nanopowdered solid solution $Ce_{1-x}Cu_xO_{2-\gamma}$ samples ($0 \leq x \leq 0.15$) were synthesized by self-propagating room temperature synthesis (SPRT). Raman spectroscopy and XRD at room temperature were used to study the vibration properties of these materials as well as the Cu solubility in ceria lattice. The solubility limit of Cu^{2+} in CeO_2 lattice was found to be lower than published in the literature. Results show that obtained powders with low dopant concentration are solid solutions with a fluorite-type crystal structure. However, with Cu content higher than 7.5 mass%, the phase separation was observed and two oxide phases, CeO_2 and CuO, coexist. All powders were nanometric in size with high specific surface area.

Keywords: D. CeO_2; Solid solution; Raman spectroscopy; XRD measurements

1. Introduction

Ceria based materials have become one of the most interesting ceramic from both materials fundamental and practical point of view. There is a number of important uses such as an electrolyte material for solid oxide fuel cells (SOFC), gas sensor, automobile exhaust catalyst, as mechanical polishing medium, as additive to other high-tech ceramics [1–4]. Especially ceria solid solution has been acknowledged to be most promising catalysts for various reactions such as the combustion of CO and methane, the reduction of SO_2, methanol synthesis and wet oxidation of phenol [5–7]. These applications of CeO_2 emerge from its reversible oxygen storage and release capacity. However, the key factor in the design of modified ceria is the choice of dopant elements, as well as their introduced amount. In addition, the method of the powder preparation has also very strong influence on the homogeneity and stability of the solid solutions.

The conventional solid state reaction method involves mixing of CeO_2 and oxides containing corresponding dopant elements. Due to low diffusion coefficients of dopant ions, prolonged heating of the mixture at elevated temperature is necessary to form the desired single-phase compounds. Moreover, in some cases the repetition of cycle consisting of heating, cooling and grinding of mixture is the only way to terminate the solid state reaction and form single-phase compounds. Furthermore, an important drawback of prolonged heat treatment at high temperature is an inevitable crystal growth and consequent decrease in surface area of the powders. From the electrical conductivity view point it is essential to obtain fine powder of ceria based material as it leads to formation of small grains after sintering. It is well documented that the conductivity in nanocrystalline grain boundary regions increases with a decrease in grain size [8]. Bearing this in mind it is important to develop powders of high quality with particle size in the nanometre range. Various methods such as glycine nitrate procedure, template-based homogenous precipitations, decomposition of oxalate precursors, sol–gel, hydrothermal route and mechanical milling reaction have been used [9–13] for the preparation of ceria and its solid solution nanoparticles.

One of the methods that are cost and time effective is the self-propagating room temperature (SPRT) synthesis of powders. The SPRT procedure is based on the self-propagating room temperature reaction between metal nitrates and sodium hydroxide. This reaction is spontaneous and terminates extremely fast [14]. Although, this method had been used

* Corresponding author. Tel.: +381 113408224; fax: +381 113408224.
E-mail address: babicb@vinca.rs (B.M. Babić).

0272-8842/$36.00
doi:10.1016/j.ceramint.2011.03.078

for synthesis of solid solution of ceria with various ions (Ba^{2+}, Y^{3+}, Ln^{3+}, Sm^{3+}, Gd^{3+}, Nd^{3+}) in different concentrations [15–18], no work has been done on preparation of Cu doped ceria.

It was found that nanosized doped ceria with copper can improve some catalytic performances compared to the industrial Cu/ZnO catalysts [19]. High activity and low cost of the copper oxide-based catalysts make them suitable substitutes for noble metal catalysts in emission control application for novel, clean fuels [20]. It is anticipated that, with proper development, copper-promoted ceria catalysts could realize much higher CO conversion than the commercial ones. It is very important to know the maximum solubility of Cu^{2+} in ceria crystal lattice.

Therefore, in the present study, we report a SPRT method for preparation of nano-crystalline powders of ceria and Cu-doped ceria. Special attention is given to study on XRD and Raman spectroscopy as well as porosity of synthesized samples.

2. Experimental

For experimental work cerium and copper nitrates were used in the reaction with sodium hydroxide. The used nitrates were p.a. compound (Aldrich, Germany) and all in the form of hexahydrates. The compositions of the starting reacting mixtures were calculated according to the nominal composition of the reaction products. Ceria doped powders were synthesized by SPRT method according to reaction:

$$2\cdot[(1-x)Ce(NO_3)_3\cdot 6H_2O + xCu(NO_3)_3\cdot 6H_2O] + 6NaOH + (1/2-\gamma)O_2 \rightarrow 2Ce_{1-x}Cu_xO_{2-\gamma} + 6NaNO_3 + 15H_2O \quad (1)$$

The following compositions were prepared: CeO_2, $Ce_{0.95}Cu_{0.05}O_{2-\gamma}$, $Ce_{0.929}Cu_{0.075}O_{2-\gamma}$, $Ce_{0.9}Cu_{0.1}O_{2-\gamma}$, $Ce_{0.875}Cu_{0.125}O_{2-\gamma}$, $Ce_{0.85}Cu_{0.15}O_{2-\gamma}$. During SPRT synthesis hand-mixing of nitrates with NaOH was performed in alumina mortar for up to 10 min until the mixture got light brown. After being exposed to air for 4 h, the mixture was suspended in water. Rinsing out of $NaNO_3$ was performed in centrifuge—Centurion 1020D, at 3500 rpm for 10 min. This procedure was repeated three times with distilled water and twice with ethanol [14].

Adsorption and desorption isotherms of N_2 were measured on samples at −196 °C using the gravimetric McBain method. From the isotherms, the specific surface area, S_{BET}, pore size distribution, mesopore including external surface area, S_{meso} and micropore volume, V_{mic}, for the samples were calculated. Pore size distribution was estimated by applying BJH method [21] to the desorption branch of isotherms and mesopore surface and micropore volume were estimated using the high-resolution α_s plot method [21–23]. Micropore surface, S_{mic}, was calculated by subtracting S_{meso} from S_{BET}.

XRD patterns of all the powders including the samples heat treated at different temperatures were recorded on Siemens X-ray Diffractometer (Kristaloflex 500) with Ni filtered Cu K_α radiation and using Si as an external standard. The measurements were performed in the range 20–80° 2θ in a continuous scan mode with a step width of 0.02° and at a scan rate of 1° 2θ/min.

Unpolarized micro-Raman scattering measurements were performed in the backscattering configuration using Jobin Yvon T64000 spectrometer equipped with nitrogen cooled Symphony® charge-coupled-device detector (CCD). As an excitation source we used 514.5-nm line of Ar-ion laser operating at low power ∼10 mW in order to avoid sample heating.

3. Results and discussion

Typical X-ray diffraction patterns for the Cu doped CeO_2 with different dopant concentrations are shown in Fig. 1. Peaks related to isolated Cu-phases are not observed and all of solid solution powders exhibit the fluorite crystal structure. XRD analysis reveals that all peaks for each sample were significantly broadened indicating small crystallite size and/or strain. It is especially true for powder with low dopant concentration ($x < 0.1$). It exhibits very diffuse diffraction lines, in such way that it is impossible to indicate some atomic planes (*h k l*: 2 0 0, 4 0 0, 3 1 1, 4 2 0). This behaviour can be ascribed to the existence of the microstrain field originated from the defect such as vacancy clusters formed due to presence of Ce^{3+} [24]. Since Cu^{2+} ions are substituted for Ce^{4+} ions and accordingly, there is an increase in the oxygen vacancy with the increase in Cu^{2+} ion substitution. Thus, oxide ion vacancy leads to an increase in the lattice parameter showing a significant broadening of peaks. Fig. 1 also shows that an increase in concentration of copper increases the intensity of diffraction peaks and sharpens diffraction lines.

This behaviour can be explained by copper segregation on the crystallite surfaces, which could not be detected by XRD. Thus, the solubility limit of copper into ceria crystal lattice may be lower than shown by literature data [25]. That is why we analysed the obtained powders by Raman spectroscopy, which is more sensitive to the local structure ordering than XRD (Figs. 2 and 3).

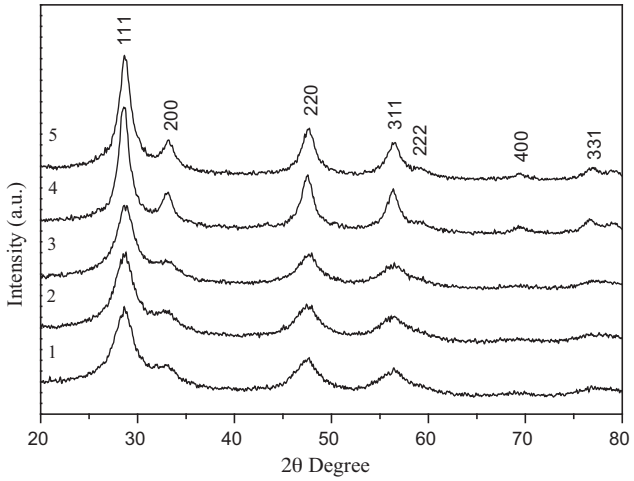

Fig. 1. X-ray diffraction patterns of $Ce_{1-x}Cu_xO_{2-\gamma}$ powders (1—5%; 2—7.5%; 3—10%; 4—12.5%; 5—15%).

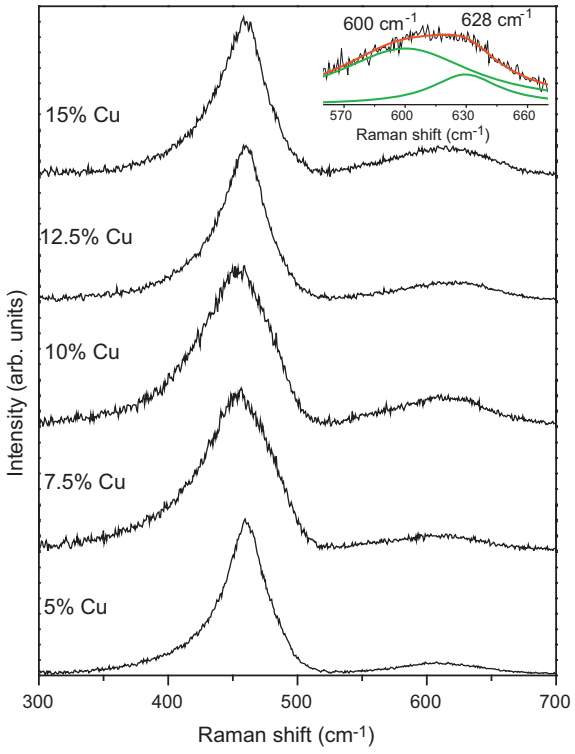

Fig. 2. Room-temperature Raman spectra of $Ce_{1-x}Cu_xO_{2-\gamma}$ nanopowders, excited by 514 nm radiation, from an argon ion laser.

In the first order Raman spectra for the low Cu concentrations ($x = 0.025$) two modes at 459 and 600 cm^{-1} are presented. The Raman mode at ~459 cm^{-1} is assigned to the F_{2g} mode of CeO_2 fluorite structure [26]. The F_{2g} mode in $Ce_{1-x}Cu_xO_{2-\gamma}$ samples shifts to the lower frequencies with an increase in of dopant concentration up to 7.5% Cu. As Fig. 2 shows, the shifts followed by an increase of mode bandwidth. This mode presents symmetrical stretching vibrations of CeO_8 vibration unit and should be very sensitive to the oxygen sublattice disorder and change of local environment with doping [27]. Additional mode, located at 600 cm^{-1}, is ascribed to intrinsic oxygen vacancies in the ceria lattice [28]. Intensity of oxygen vacancy mode increases with doping content up to 7.5% as well. In the Raman spectrum of 7.5% Cu-doped ceria new mode appears new mode at ~628 cm^{-1}, which is ascribed to B_g Raman mode characteristic for nanocrystalline CuO structure [29]. The inset presents the part of the Raman spectrum of 7.5% Cu-doped ceria where CuO and oxygen vacancy modes are fitted by Lorentzian type profile. Further increase of Cu content leads to F_{2g} mode frequency blueshift and bandwidth decrease and distinct appearance of CuO mode. From Raman scattering results we have concluded that these compounds are solid solutions in low doping regime (up to 7.5% Cu). With increasing Cu content the phase separation begins where two oxide systems CeO_2 and CuO coexist.

The difference between surface layer and bulk of nanocrystalline samples can be studied by Raman spectroscopy using different laser excitation lines. It is well known that Raman spectroscopy with shorter excitation (514 nm) is more surfaces sensitive while longer wavelength (647 nm) gives more information about the particle bulk.

To obtain the information about the defect distribution in bulk and surface layer of $Ce_{1-x}Cu_xO_{2-\gamma}$ samples doped with higher Cu content ($x \geq 7.5\%$) we performed Raman measurements with 647 nm line was performed as well.

The Raman spectra of two samples doped with 7.5% and 15% of Cu using 647 nm laser lines are presented in Fig. 3. As can be seen, in the sample with lower Cu content only F_{2g} Raman mode is presented whereas in the 15% Cu-doped sample there is an evidence of the Raman mode, which belongs to oxygen vacancy modes (designated with * in Fig. 3). The mode which belongs to CuO was not observed. From this study we concluded that in samples with lower Cu concentration (7.5%) the defect states and CuO layer are mainly distributed in the surface layer of nanoparticles. However, for higher dopant concentrations a fraction of the oxygen defect states is also distributed in the particle bulk.

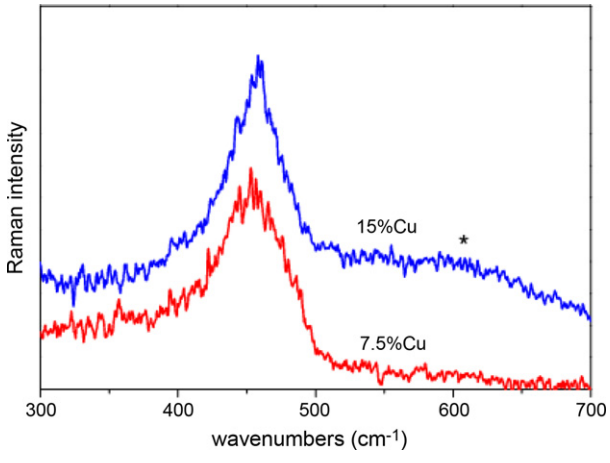

Fig. 3. Room-temperature Raman spectra of $Ce_{1-x}Cu_xO_{2-\gamma}$ ($x = 7.5\%$ and 15% Cu) nanopowders excited by 647 nm radiation from an argon ion laser.

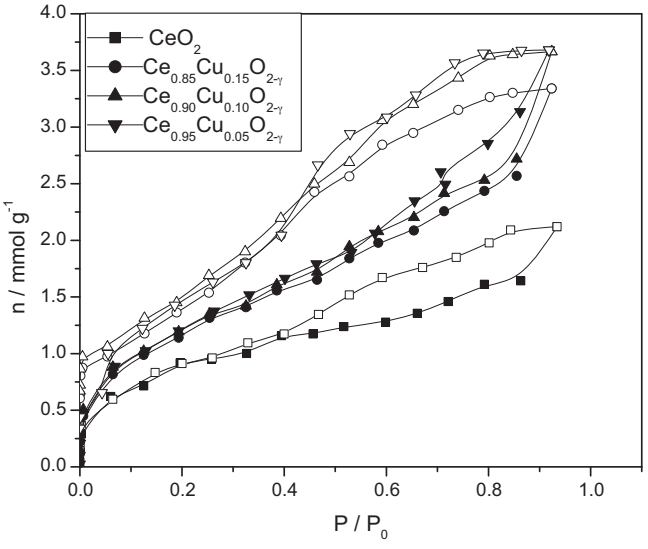

Fig. 4. Nitrogen adsorption isotherms for CeO_2 sample and samples of CeO_2 with different amount of Cu. Solid symbols—adsorption, open symbols—desorption.

Table 1
Porous properties of samples.

Sample	S_{BET} (m^2/g)	S_{meso} (m^2/g)	S_{mic} (m^2/g)	V_{mic} (cm^3/g)
CeO_2	70	45	25	0.013
$Ce_{0.85}Cu_{0.15}O_{2-\gamma}$	94	85	9	0.006
$Ce_{0.90}Cu_{0.10}O_{2-\gamma}$	97	93	4	0.004
$Ce_{0.95}Cu_{0.05}O_{2-\gamma}$	98	90	8	0.012

Nitrogen adsorption isotherms, as the amount of N_2 adsorbed as function of relative pressure at −196 °C, are shown in Fig. 4. According to the IUPAC classification isotherms are of type-IV and with a hysteresis loop, which is associated with mesoporous materials. Fig. 4 shows CeO_2 sample and samples of CeO_2 with different amount of Cu. Specific surface areas calculated by BET equation, S_{BET}, are listed in Table 1. S_{BET} value for CeO_2 sample is 70 m^2/g, and the values for CeO_2 with different amount of Cu are between 90 and 100 m^2/g. Although the presence of Cu increases the specific surface, S_{BET} does not change with changing the amount of Cu in samples.

Pore size distribution of CeO_2 sample and samples of CeO_2 with different amount of Cu is shown in Fig. 5. One can see that samples have a similar pore size distribution. The radius of pores varies between 2 and 6 nm, which means that all samples are mostly mesoporous according to IUPAC classification (micropores ≤ 2 nm, mesopores 2–50 nm and macropores ≥ 50 nm).

α_s plots, obtained on the basis of the standard nitrogen adsorption isotherm are shown in Fig. 6. The straight line in the medium α_s region gives a mesoporous surface area including the contribution of external surface, S_{meso}, determined by its slope, and micropore volume, V_{mic}, is given by the intercept. The calculated porosity parameters (S_{meso}, S_{mic}, V_{mic}) are given in Table 1. Table 1 shows that the presence of Cu increases mesoporous surfaces and decreases microporous surface and volume. The amount of Cu does not influence mesoporous surfaces and microporous surface and volume.

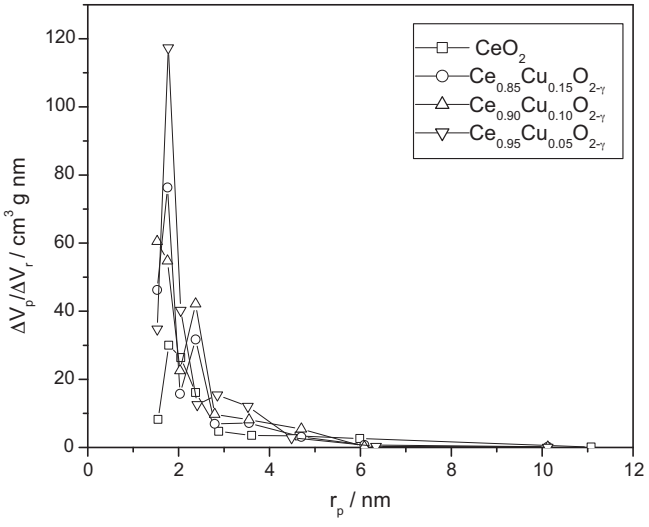

Fig. 5. Pore size distribution (PSD) of CeO_2 sample and samples of CeO_2 with different amount of Cu.

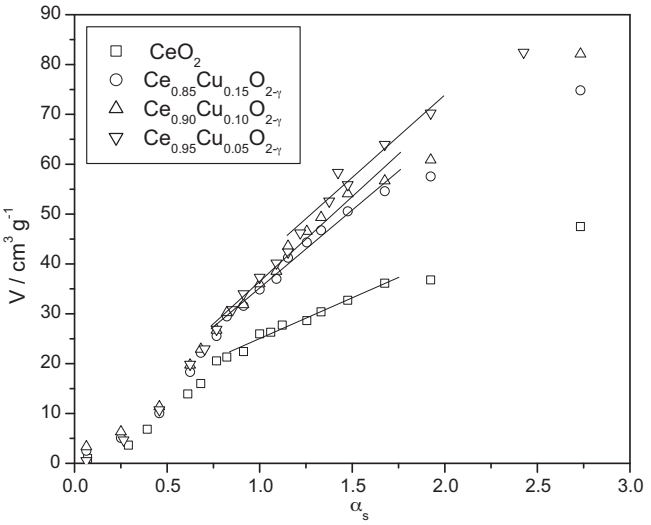

Fig. 6. α_S—plots for nitrogen adsorption isotherm of CeO_2 sample and samples of CeO_2 with different amount of Cu.

4. Conclusion

SPRT method was applied to produce Cu doped ceria nanoparticles with an average crystalline size of 4 nm. The results indicate that not more than 7.5 mass% of copper can be incorporated to the Ce^{4+} sites of $Ce_{1-x}Cu_xO_{2-\gamma}$. Any further addition of copper results in the formation of a second phase, i.e. CuO. However, all powders exhibited high surface area with meso- and microporosity. The presence of copper increases the specific surface area (∼100 m^2/g) compared to pure ceria (70 m^2/g).

Acknowledgement

The Ministry of Science of Serbia financially supported this project (No. 45012).

References

[1] A. Trovarelli, C. de Leiterburg, M. Boaro, G. Dolcetti, The utilization of ceria in industrial catalysis, Catal. Today 50 (1999) 353–367.
[2] D. Waller, J.A. Lane, J.A. Kilner, B.C.H. Steele, The effect of thermal treatment on the resistance of LSCF electrodes on gadolinia doped ceria electrolytes, Solid State Ionics 86 (1996) 767–772.
[3] U. Lampe, J. Gerblinger, H. Meixner, Comparison of transient response of exhaust-gas sensors based on thin films of selected metal oxides, Sens. Actuators B 7 (1992) 787–791.
[4] A. Tsoga, A. Gupta, A. Naoumidis, P. Nikolopoulos, Gadolinia-doped ceria and yttria stabilized zirconia interfaces: regarding their application for SOFC technology, Acta Mater. 48 (2000) 4709–4714.
[5] P.G. Harrison, I.K. Ball, W. Azelee, W. Daniel, D. Goldfarb, Nature and surface redox properties of copper(II)-promoted cerium(IV) oxide CO-oxidation catalysts, Chem. Mater. 12 (2000) 3715–3725.
[6] W. Shan, W. Shen, C. Li, Structural characteristics and redox behaviors of $Ce_{1-x}Cu_xO_y$ solid solutions, Chem. Mater. 15 (2003) 4761–4767.
[7] X. Wang, J.A. Rodriguez, J.C. Hanson, D. Gamarra A., M. Martinez-Arias, Fernandez-Garcia, Unusual physical and chemical properties of Cu in $Ce_{1-x}Cu_xO_2$ oxides, J. Phys. Chem. B 109 (2005) 19595–19603.
[8] L.A. Chick, G.D. Maupin, L.R. Pederson, Glycine-nitrate synthesis of a ceramic-metal composite, Nanostruct. Mater. 4 (1994) 603–615.

[9] Y.H. Li, X.Z. Zhou, Y. Wang, X.Z. You, Preparation and properties of Ni/YSZ anode by coating precipitation method, Mater. Lett. 58 (2004) 3079–3083.
[10] Y.J. Wang, J.M. Ma, M.F. Luo, P. Fang, M. He, Preparation of high-surface area nano-CeO_2 by template-assisted precipitation method, J. Rare Earths 25 (2007) 58–62.
[11] J. Wang, O. Liu, Q. Liu, Ceria- and Cu-doped ceria nanocrystals synthesized by the hydrothermal methods, J. Am. Ceram. Soc. 91 (2008) 2706–2708.
[12] S. Boskovic, S. Zec, M. Ninic, J. Dukic, B. Matovic, D. Djurovic, F. Aldinger, Nanosized ceria solid solutions obtained by different chemical routes, J. Optoelectron. Adv. Mater. 10 (2008) 515–519.
[13] M.F. Luo, J.M. Ma, J.Q. Lu, Y.P. Song, Y.J. Wang, High-surface area CuO–CeO_2 catalysts prepared by a surfactant-templated method for low-temperature CO oxidation, J. Catal. 246 (2007) 52–59.
[14] S. Boskovic, D. Djurovic, S. Zec, B. Matovic, M. Zinkevich, F. Aldinger, Doped and Co-doped CeO_2: preparation and properties, Ceram. Int. 34 (2008) 2001–2006.
[15] Z.D. Dohcevic-Mitrovic, M.J. Scepanovic, M.U. Grujic-Brojcin, Z.V. Popovic, B.Z. Matovic, S.B. Boskovic, Temperature-dependent Raman study of $Ce_{0.75}Nd_{0.25}O_{2-\delta}$ nanocrystals, Appl. Phys. Lett. 91 (2007) 203118–203121.
[16] M. Radovic, Z. Dohcevic-Mitrovic, M. Scepanovic, M. Grujic-Brojcin, B. Matovic, S. Boskovic, Z.V. Popovic, Raman study of Ba-doped ceria nanopowders, Sci. Sintering 39 (2007) 281–286.
[17] M. Ninic, S. Boskovic, M. Nenadovic, S. Zec, K. Voisavljevic, D. Minic, B. Matovic, Cerium oxide based nanometric powders: synthesis and characterization, Sci. Sintering 39 (2007) 301–308.
[18] B. Matovic, J. Dukic, A. Devecerski, S. Boskovic, M. Ninic, Z. Dohcevic-Mitrovic, Crystal structure analysis of Nd-doped ceria solid solutions, Sci. Sintering 40 (2008) 63–68.
[19] Y. Liu, T. Hayakama, K. Suzuki, S. Hamakawa, Production of hydrogen by steam reforming of methanol over Cu/CeO_2 catalysts derived from $Ce_{1-x}Cu_xO_{2-x}$ precursors, Catal. Commun. 2 (2001) 195–200.
[20] J. Papvasiliou, G. Avgouropoulos, T. Ioannides, Production of hydrogen via combined steam reforming of methanol over CuO–CeO_2 catalysts, Catal. Commun. 5 (2004) 231–235.
[21] E.P. Barret, L.G. Joyner, P.P. Halenda, The determination of pore volume and area distributions in porous substances. I. Computations from nitrogen isotherms, J. Am. Chem. Soc. 73 (1951) 373–380.
[22] K. Kaneko, C. Ishii, M. Ruike, H. Kuwabara, Origin of superhigh surface area and microcrystalline graphitic structures of activated carbons, Carbon 30 (1992) 1075–1088.
[23] M. Kruk, M. Jaroniec, K.P. Gadakaree, Nitrogen adsorption studies of novel synthetic active carbons, J. Colloid Interface Sci. 192 (1997) 250–256.
[24] W. Qin, Z.H. Chen, P.Y. Huang, Y.H. Zhuang, Crystal lattice expansion of nanocrystalline materials, J. Alloys Compd. 292 (1999) 230–232.
[25] A. Gayen, K.R. Priolkar, A.K. Shukla, N. Ravishankar, M.S. Hegde, Oxide-ion conductivity in $Cu_xCe_{1-x}O_{2-\delta}$ ($0 \leq x \leq 0.10$), Mater. Res. Bull. 40 (2005) 421–431.
[26] W.H. Weber, K.C. Hass, J.R. McBride, Raman study of $CerO_2$: second order scattering, lattice dynamics, and particle size effects, Phys. Rev. B 48 (1993) 178–185.
[27] I. Kosacki, T. Suzuki, H. Anderson, P. Colomban, Raman scattering and lattice defects in nanocrystalline CeO_2 thin films, Solid State Ionics 149 (2002) 99–105.
[28] A. Nakajima, A. Yoshihara, M. Ishigame, Defect-induced Raman spectra in doped CeO_2, Phys. Rev. B 50 (1994) 13297–13307.
[29] Z.V. Popovic, C. Thomsen, M. Cardona, R. Liu, G. Stanisic, R. Kremer, W. König, Phonon characterization of Bi_2 $(Sr_{1-x}Ca_x)_2$ $CuO_{6+\delta}$ by infrared and Raman spectroscopy, Solid State Commun. 66 (1988) 965–969.